Journal of Solid State Chemistry 181 (2008) 2755–2762

Contents lists available at ScienceDirect

Journal of Solid State Chemistry

journal homepage: www.elsevier.com/locate/jssc

Formation and structural refinements of tunneled intergrowth phases in the Ga_2O_3–In_2O_3–SnO_2–TiO_2 system

C.R. Maier, M. Charoenwongsa, D.D. Edwards *

Kazuo Inamori School of Engineering, Alfred University, 2 Pine Street, Alfred, NY 14802, USA

ARTICLE INFO

Article history:
Received 31 March 2008
Received in revised form
16 June 2008
Accepted 20 June 2008
Available online 3 July 2008

Keywords:
Beta-gallia
Rutile
Intergrowth
One-dimensional tunnel

ABSTRACT

Over 100 samples were prepared as $(Ga,In)_4(Sn,Ti)_{n-4}O_{2n-2}$, $n=6$, 7, and 9 by solid-state reaction at 1400 °C and characterized by X-ray diffraction. Nominally phase-pure beta-gallia–rutile intergrowths were observed in samples prepared with $n=9$ ($0.17\leqslant x\leqslant 0.35$ and $0\leqslant y\leqslant 0.4$) as well as in a few samples prepared with $n=6$ and 7. Rietveld analysis of neutron time-of-flight powder diffraction data were conducted for three phase-pure samples. The $n=6$ phase $Ga_{3.24}In_{0.76}Sn_{1.6}Ti_{0.4}O_{10}$ is monoclinic, $P2/m$, with $Z=2$ and $a=11.5934(3)$ Å, $b=3.12529(9)$ Å, $c=10.6549(3)$ Å, $\beta=99.146(1)^\circ$. The $n=7$ phase $Ga_{3.24}In_{0.76}Sn_{2.4}Ti_{0.6}O_{12}$ is monoclinic, $C2/m$, with $Z=2$ and $a=14.2644(1)$ Å, $b=3.12751(2)$ Å, $c=10.6251(8)$ Å, $\beta=108.405(1)^\circ$. The $n=9$ phase $Ga_{3.16}In_{0.84}Sn_4TiO_{16}$ is monoclinic, $C2/m$, with $Z=2$ $a=18.1754(2)$ Å, $b=3.13388(3)$ Å, $c=10.60671(9)$ Å, $\beta=102.657(1)^\circ$. All of the structures are similar in that they possess distorted hexagonal tunnels parallel to the [010] vector.

1. Introduction

Tunneled intergrowth structures form upon the high-temperature interaction between β-gallia (Ga_2O_3) and metal oxides that crystallize in the rutile structure. The resultant intergrowth structures characteristically adopt a monoclinic cell and a short unit cell b vector, ~3 Å, both of which are derived from the parent β-gallia structure. The series of beta-gallia–rutile (BGR) intergrowth phases may be expressed generically as $Ga_4M_{n-4}O_{2n-2}$, where MO_2 is an oxide that crystallizes in the rutile structure (SnO_2, TiO_2, or GeO_2) and n is an integer ($5\leqslant n<\infty$) [1–9].

The BGR phases are coherent intergrowths of the beta-gallia and rutile structures in such a manner that [010] beta-gallia is parallel to [001] rutile—both of which are parallel to [010] of the intergrowth structure. Depending on how the β-gallia and rutile sub-units are arranged, two distinct homologous series result [5,6]. In one series, the integer n assumes only odd values, and the resulting structures can be described in terms of a (210) $[\frac{1}{2},\frac{1}{4},\frac{1}{2}]$ crystallographic shear plane (CSP) operation on the parent rutile structure. In the other series, the integer n assumes both odd and even values, and the resulting structures can be described in terms of a (210) $[0,\frac{1}{2},0]$ CSP operation on the rutile structure. Based on the CSP descriptions, the $n=5$ member can be considered a member of both series, but is more appropriately associated with the $n=$ odd series since it adopts a $C2/m$ symmetry that is characteristic of the members in this series. $P2/m$ symmetry is observed in the series that can adopt both odd and even n integers ($n\geqslant 6$).

Intergrowth stability varies with composition and temperature. In the Ga_2O_3–TiO_2 system, several members with $5<n<51$ (odd) have been observed [1,2], and the number of thermodynamically stable intergrowths increases with increasing temperature. In the Ga_2O_3–GeO_2 system, only the $n=5$ and 7 ($C2/m$) members have been observed [3]. In the Ga_2O_3–SnO_2 system, the $n=5$ member occurs above 1300 °C [4]. Substitution of indium for gallium in the Ga_2O_3–SnO_2 system, results in the stabilization of $n=6$ and 7 ($P2/m$) structures as well as $9<n<17$ ($C2/m$) structures [5,6].

A unifying feature of all of these phases is the presence of distorted hexagonal tunnels parallel to [010] of the intergrowth structure. The tunnels are suitable hosts for alkali cations as has been demonstrated in the one-dimensional ionic conductor, $Na_xGa_{4+x}Ti_{1-x}O_8$, $x\cong 0.7$, which is a derivative of the $n=5$ intergrowth [7–9]. BGR intergrowths prepared without cations in the tunnel may be potential candidates for ion-storage applications, such as Li-ion battery electrodes, providing that a sufficient amount of reducible cations, like $Ti^{4+/3+}$, can be incorporated into low-n (high-tunnel-density) intergrowths.

In the current investigation, we have prepared low-n Ti-containing intergrowths by substituting Ti for Sn in $n=6$, 7, and 9 intergrowths known to exist in the Ga_2O_3–In_2O_3–SnO_2 system. We hypothesized that intergrowth stability in the Ga_2O_3–In_2O_3–SnO_2–TiO_2 system would be related to the degree of matching between the [010] lattice vector of the $(Ga,In)_2O_3$

* Corresponding author. Fax: +1 607 871 3047.
E-mail address: dedwards@alfred.edu (D.D. Edwards).

0022-4596/$ - see front matter © 2008 Elsevier Inc. All rights reserved.
doi:10.1016/j.jssc.2008.06.055

component and the [001] lattice vector of the $(Sn,Ti)O_2$ component. This hypothesis was based on the observation that many intergrowth structures are stable in the Ga_2O_3–TiO_2 system where the lattice mismatch is 2.7% and that few intergrowth structures are stable in the Ga_2O_3–GeO_2 and Ga_2O_3–SnO_2 systems where the lattice mismatch is higher at 5.9% and 4.8%, respectively. The hypothesis is further supported by the fact that In substitutions for Ga, which decrease the lattice mismatch between $(Ga,In)_2O_3$ and SnO_2, result in the stabilization of several intergrowths not seen in the Ga_2O_3–SnO_2 system [5,6].

In this paper, the factors which influence intergrowth formation in the Ga_2O_3–In_2O_3–SnO_2–TiO_2 are discussed. Additionally, we report on the refinement of three $(Ga,In)_4(Sn,Ti)_{n-4}O_{2n-2}$ structures. The structures for ($n=6$) $Ga_{4-4x}In_{4x}Sn_{2-2y}Ti_{2y}O_{10}$, and ($n=7$) $Ga_{4-4x}In_{4x}Sn_{3-3y}Ti_{3y}O_{12}$ have been refined using neutron powder diffraction data, while the structure of the ($n=9$) $Ga_{4-4x}In_{4x}Sn_{5-5y}Ti_{5y}O_{16}$ has been determined for the first time using a combination of X-ray and neutron powder diffraction.

2. Experimental

Specimens were prepared from oxide powders (all >99.9% purity, metals basis), that had been dried in a drying oven overnight and stored in a dessicator prior to batching to remove absorbed moisture. Samples were prepared as $Ga_{4-4x}In_{4x}Sn_{2-2y}Ti_{2y}O_{10}$ ($n=6$), $Ga_{4-4x}In_{4x}Sn_{3-3y}Ti_{3y}O_{12}$ ($n=7$), and $Ga_{4-4x}In_{4x}Sn_{5-5y}Ti_{5y}O_{16}$ ($n=9$). All reagents were weighed to the nearest 0.0001 g, homogenized in an agate mortar and pestle, and pressed into a pellet prior to heating. The pellets were placed into sacrificial powder beds of the same composition in covered Al_2O_3 crucibles and heated at 1250 °C for 2 days, after which the pellets were ground into a powder, repressed into pellets, and heated at 1400 °C for 7–40 days with intermediate grinding and X-ray characterization after dry quenching in ambient air. Heating was discontinued when the samples were deemed phase pure or after no further changes were observed in the X-ray diffraction patterns.

Three nominally phase-pure samples—prepared with $n=6$, 7, and 9 and with $x=0.19$ and $y=0.2$—were selected for further structural investigations. The lattice constants of each sample were determined by placing a monolayer of powder onto a non-diffracting polished quartz single-crystal to eliminate errors in peak position owing to sample transparency. The systematic error in the position of the diffraction maxima was corrected for by analyzing a sample of NIST srm640b standard prepared in an identical fashion. In all cases, data were collected over a range of 5–80° 2θ at a step size of 0.02° 2θ, and dwell time of 20 s to improve counting statistics. The lattice constants were refined using a software program (MDI, Jade), which utilizes least-squares methods. Time-of-flight neutron diffraction data for all three specimens were acquired at the Argonne National Laboratory's Intense Pulse Neutron Source (IPNS). Rietveld refinements were conducted using GSAS with the EXPGUI graphical front-end [10,11]. Corrections were applied for container scattering angle-dependent absorption, but were not allowed to refine. Scattering factors for Ga, In, Sn, Ti, and O were taken from the International Tables of Crystallography [12].

3. Results

3.1. Observed reaction products

Fig. 1 shows the reaction products observed in samples prepared as $(Ga,In)_4(Sn,Ti)_{n-4}O_{2n-2}$ using X-ray diffraction. In Fig. 1, the horizontal and vertical axes correspond respectively to the composition of the beta-gallia ($Ga_{2-2x}In_{2x}O_3$) and rutile ($Sn_{1-y}Ti_y$) components of the desired intergrowth oxides. The diagonal lines show the degree of lattice mismatch, defined as $(b_{gallia}-c_{rutile})\times 100/b_{gallia}$, based on the lattice parameters reported for $Ga_{2-2x}In_{2x}O_3$ and $Sn_{1-y}Ti_yO_2$ solid solutions [5,13]. The data collected in this study do not strongly support our hypothesis that phase stability depends on the degree of lattice mismatch between the β-gallia and rutile components of the structure.

For $n=6$ and 7 (Figs. 1a and b), only a few phase-pure samples were obtained. Representative X-ray diffraction patterns of the phase-pure samples are shown in Figs. 2a and b. It is interesting to note that compositions resulting in single-phase $n=6$ and 7 samples in the Ga_2O_3–In_2O_3–SnO_2 system at 1250 °C [5] were not found to be phase pure in the current study at 1400 °C.

For compositions prepared with $n=9$ (Fig. 1c), samples prepared with $0.17\leqslant x\leqslant 0.35$ were phase pure. A representative X-ray diffraction pattern is shown in Fig. 2c. In general, the unit cell volume of phase-pure $n=9$ samples increased with increasing indium content (x) and decreased with increasing titanium content (y) as expected based on the ionic radii of the cations. The X-ray diffraction patterns of samples prepared with $x=0.19$ and $y>0.4$ (not shown) indicated predominantly an $n=9$ phase with no clear evidence of other intergrowth phases. However, some of the reflections of the $n=9$ phase appeared to be split, which may result for the presence of two $n=9$ phases of different compositions.

Several observations lead us to believe that some of the phase assemblages observed may not represent the equilibrium state (quenched from 1400 °C), but may result from sluggish kinetics associated with intergrowth formation. For example, samples prepared with similar compositions and heating schedules did not always yield identical results in terms of the degree of reaction and of the presence and amount of secondary phases. One of the factors which appeared to influence the reaction was the presence of minor impurities; samples prepared with 99.9+% pure SnO_2 (containing Fe and Sb as the main impurities at <200 ppm each) reacted much more rapidly than did those prepared with 99.99+% SnO_2.

3.2. Structure refinement of $Ga_{3.24}In_{0.76}Sn_{1.6}Ti_{0.4}O_{10}$ ($n=6$)

Neutron diffraction data were collected and used for the structural refinement of an $n=6$ sample prepared as $Ga_{3.24}In_{0.76}Sn_{1.6}Ti_{0.4}O_{10}$ The atom positions reported for the $P2/m$ structure of $Ga_{2.8}In_{1.2}Sn_2O_{10}$ [6] were input as the initial positions. Starting lattice parameters were obtained from the X-ray diffraction data shown in Fig. 2a.

Fig. 3 shows the refined structure projected along [010]. There are three independent Sn/Ti sites, two edge-sharing Ga/In sites in octahedral environments, and two Ga atoms exhibiting tetrahedral symmetry. Because the M–O bond lengths associated with the tetrahedra were far too short to accommodate In atoms, it was assumed that these sites were completely occupied by Ga atoms. For the remainder of the octahedral cation sites, the site occupancy fractions for the respective atoms were set at equal starting values, such that the nominal composition of the sample was reproduced. Neither hard constraints nor soft restraints were applied. Initially the positional parameters for all atoms were allowed to vary, along with a unified U_{iso} for all oxygen atoms, and reasonably assumed U_{iso} values for all cations. Then, the site occupancy fractions for all substituted cation positions were allowed to refine in addition to the rest of the crystallographic variables. While the calculated pattern essentially provided a greatly improved fit, the U_{iso} values for one particular Sn/Ti site

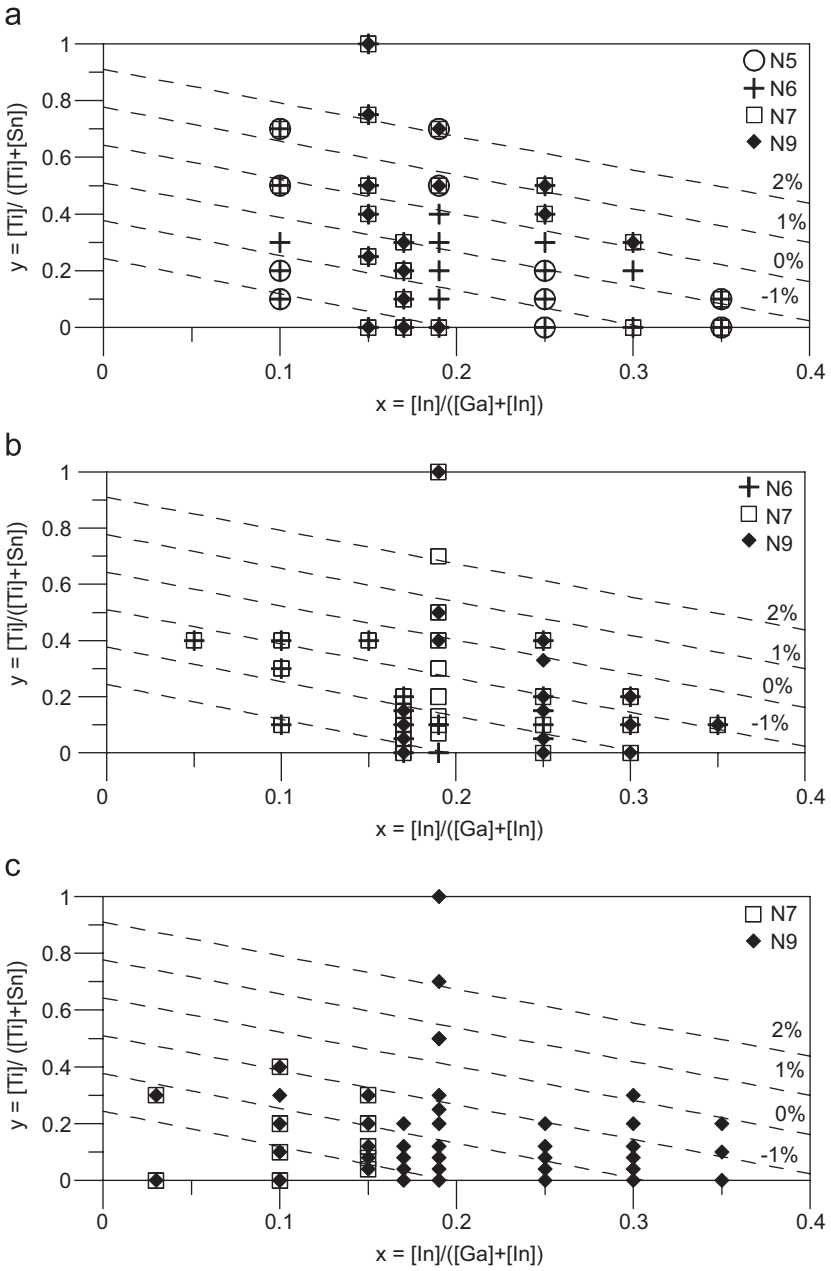

Fig. 1. Reaction products observed for samples prepared as $Ga_{4-4x}In_{4x}(Sn_{1-y}Ti_y)_nO_{2n-2}$: (a) samples prepared with $n = 6$; (b) samples prepared with $n = 7$; and (c) samples prepared with $n = 9$.

refined to values that were unacceptably dissimilar from the rest. To cope with this, an overall temperature factor was refined for the three Sn/Ti sites, in addition to the fractional occupancy of the atoms at the site. This reduced the effects of the correlation between these two variables, and produced temperature factors reasonably similar to the Ga/In sites. At this point, it was noted that the refined Sn occupancy for atoms situated at site 1*d* (0.5, 0, 0), were within one estimated standard deviation (esd) of unity. Thus, in the near-final refinement, this site was assumed to contain no substituted Ti.

Further refinements were pursued to verify that In atoms are not present on either of the two tetrahedral sites as initially assumed. The site occupancy fraction for atoms on these sites was allowed to refine (independent of their U_{iso} parameters) along with all the other structural variables, however, both sites refined to values not significantly different from unity. In the final refinement, the positional parameters for all atoms, percentage occupancy for four sites, and isotropic thermal displacement parameters were allowed to refine in addition to the lattice constants, diffractometer bank zero-correction, and a 10-term background function (Chebyschev polynomial). The final structural parameters from this refinement are tabulated in Table 1. The final χ^2 and averaged R_{wp} value for this refinement were 1.732 and 0.0436, respectively.

Bond lengths derived from the powder data are listed in Table 2. The average bond lengths for $M(1)$–O_6/$M(3)$–O_6 octahedra are on average slightly shorter than the corresponding average values for $M(2)$–O_6 octahedra. This further lends support to the notion that there is no significant occupation of (smaller) Ti atoms at the $M(2)$ sites. The occupancy fractions for Ti on $M(1)$ and $M(3)$ sites are essentially within 1 pooled esd of each other, 0.11(2) and 0.08(2), respectively. The distribution of In atoms on the $M(4)$ and $M(5)$ octahedral sites is not uniform. The majority of the In atoms reside preferentially on the $M(4)$ sites. The same result was

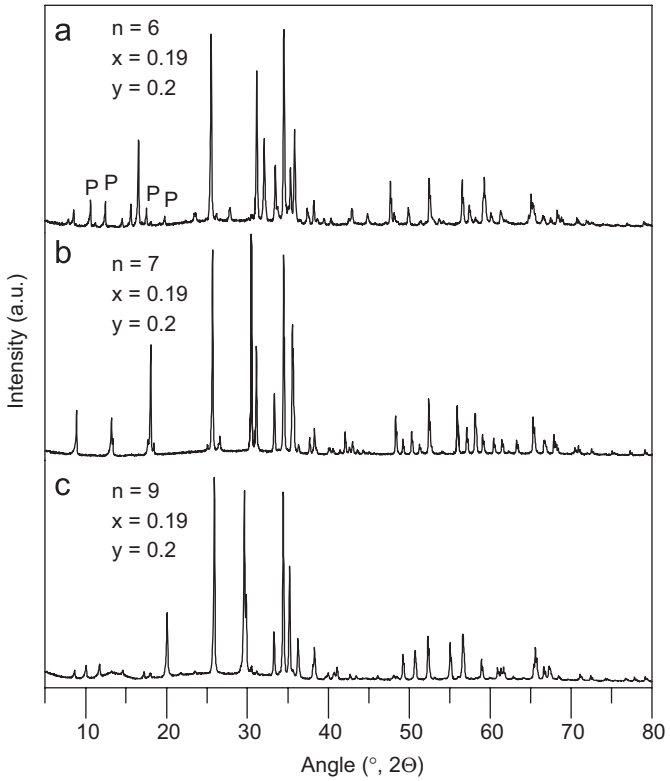

Fig. 2. X-ray diffraction patterns of samples prepared as $Ga_{4-4x}In_{4x}(Sn_{1-y}Ti_y)_nO_{2n-2}$, ($x = 0.19$, $y = 0.2$): (a) $n = 6$, (b) $n = 7$, and (c) $n = 9$. The "*P*" indicates reflections allowed by primitive ($P2/m$) symmetry assumed by the $n = 6$ sample. The $n = 7$ and 9 sample possess $C2/m$ symmetry.

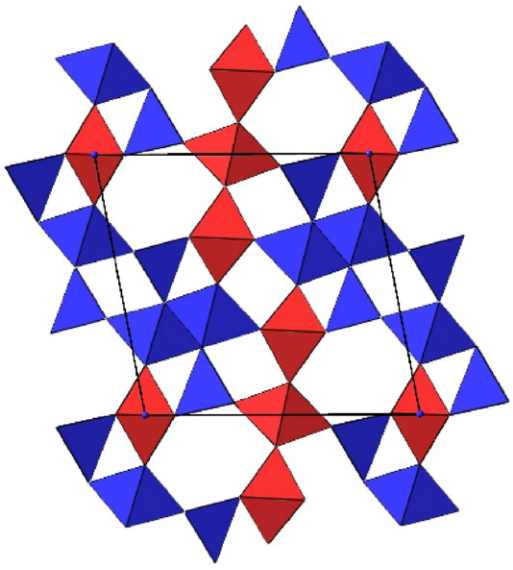

Fig. 3. Structure of $Ga_{3.24}In_{0.76}Sn_{1.6}Ti_{0.4}O_{10}$ ($n = 6$, $P2/m$) projected along [010] with the *a*-axis placed horizontally. Corner-sharing $(Sn/Ti)O_6$ octahedra shown in red. Edge sharing $(Ga,In)O_6$ octahedra and GaO_4 tetrahedra shown in blue.

observed for a sample of $Ga_{4-4x}In_{4x}SnO_8$ [6]. It is noted that the average bond length on the Ga(4) sites exceeds that of the Ga(5) sites, which is in every way consistent with the average cation radii.

The overall composition suggested by the refinement, $Ga_{2.78}In_{1.22}Sn_{1.87}Ti_{0.13}O_{10}$, is different from the as-batched composition of $Ga_{3.24}In_{0.76}Sn_{1.6}Ti_{0.4}O_{10}$. Additional refinements were conducted with various hard and soft constraints to maintain the batched composition. Acceptable refinements were obtained with $R_{wp} \cong 0.04$–0.05 and $\chi^2 \leqslant 2.0$, but all led to negative isotropic thermal parameters for some or all of the Sn/Ti sites, depending on what type of constraints were used. As an example, Fig. 4

Table 1
Structural parameters for $Ga_{3.24}In_{0.76}Sn_{1.6}Ti_{0.4}O_{10}$ ($n = 6$)[a]

Atom	Site	*x*	*y*	*z*	U_{iso}*100 Å^2	Occupancy
Sn(1)	1*a*	0	0	0	5.3(4)	0.89(2)
Ti(1)	1*a*	0	0	0	5.3(4)	0.11(2)
Sn(2)	1*d*	0.5	0	0	5.3(4)	1
Sn(3)	2*n*	0.5897(10)	0.5	0.3180(13)	5.3(4)	0.92(2)
Ti(3)	2*n*	0.5897(10)	0.5	0.3180(13)	5.3(4)	0.08(2)
Ga(4)	2*m*	0.332(8)	0	0.3892(9)	6.5(2)	0.54(3)
In(4)	2*m*	0.332(8)	0	0.3892(9)	6.5(2)	0.46(3)
Ga(5)	2*n*	0.0783(9)	0.5	0.3013(8)	7.5(3)	0.85(3)
In(5)	2*n*	0.0783(9)	0.5	0.3013(8)	7.5(3)	0.15(3)
Ga(6)	2*m*	0.1469(6)	0	0.5990(6)	0.3(2)	1
Ga(7)	2*n*	0.2621(6)	0.5	0.0810(8)	4.8(2)	1
O(1)	2*m*	0.3320(9)	0	0.0454(14)	3.4(4)	1
O(2)	2*m*	0.0361(9)	0	0.1923(11)	2.4(5)	1
O(3)	2*m*	0.4806(8)	0	0.3279(9)	0.9(5)	1
O(4)	2*m*	0.7136(9)	0	0.3149(10)	4.6(5)	1
O(5)	2*m*	0.1493(8)	0	0.4294(9)	1.7(4)	1
O(6)	2*n*	0.1056(9)	0.5	−0.0042(12)	3.2(5)	1
O(7)	2*n*	0.5469(10)	0.5	0.1212(13)	3.8(5)	1
O(8)	2*n*	0.2529(8)	0.5	0.2593(12)	3.1(4)	1
O(9)	2*n*	0.3556(7)	0.5	0.5030(10)	3.9(4)	1
O(10)	2*n*	0.0725(9)	0.5	0.6298(10)	2.4(4)	1
		h *k l*		R_{wp}		R_p
Bank 1		110		0.0460		0.0375
Bank 2		55		0.0399		0.0333
Bank 3		13		0.0374		0.0351
Totals		178		0.0436		0.0359
χ^2		1.732				

[a] Space group $P2/m$, $a = 11.5934(3)$Å, $b = 3.12529(9)$Å, $c = 10.6549(3)$Å, $\beta = 99.146(1)^\circ$.

Table 2
Bond lengths in $Ga_{3.24}In_{0.76}Sn_{1.6}Ti_{0.4}O_{10}$ ($n = 6$)

Polyhedra	Bond		Number	Length (Å)
$(Sn/Ti)O_6$	Sn(1)/Ti(1)	–O(2)	2	2.025(12)
		–O(6)	4	1.990(6)
SnO_6	Sn(2)	–O(1)	2	2.080(11)
		–O(7)	4	2.045(9)
$(Sn/Ti)O_6$	Sn(3)/Ti(3)	–O(3)	2	2.024(9)
		–O(4)	2	2.126(12)
		–O(7)	1	2.077(17)
		–O(9)	1	1.912(12)
$(Ga/In)O_6$	Ga(4)/In(4)	–O(3)	1	1.935(12)
		–O(5)	1	2.228(13)
		–O(8)	2	2.190(11)
		–O(4)	2	1.970(9)
$(Ga/In)O_6$	Ga(5)/In(5)	–O(2)	2	1.962(8)
		–O(5)	2	2.151(10)
		–O(8)	1	2.141(14)
		–O(10)	1	2.002(13)
GaO_4	Ga(6)	–O(4)	1	1.728(13)
		–O(5)	1	1.811(12)
		–O(10)	2	1.839(6)
GaO_4	Ga(7)	–O(1)	2	1.828(6)
		–O(6)	1	1.896(13)
		–O(8)	1	1.920(15)

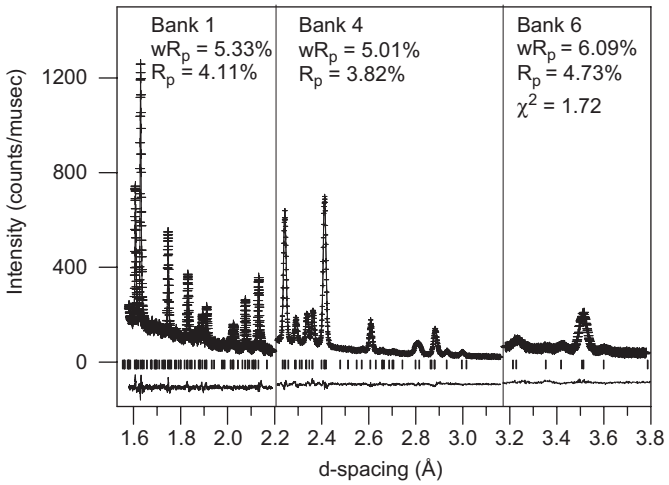

Fig. 4. Observed (+), calculated (line), and difference patterns for $Ga_{3.24}In_{0.76}Sn_{1.6}Ti_{0.4}O_{10}$. Rietveld analysis of neutron diffraction data was conducted using hard and soft constraints to maintain original composition.

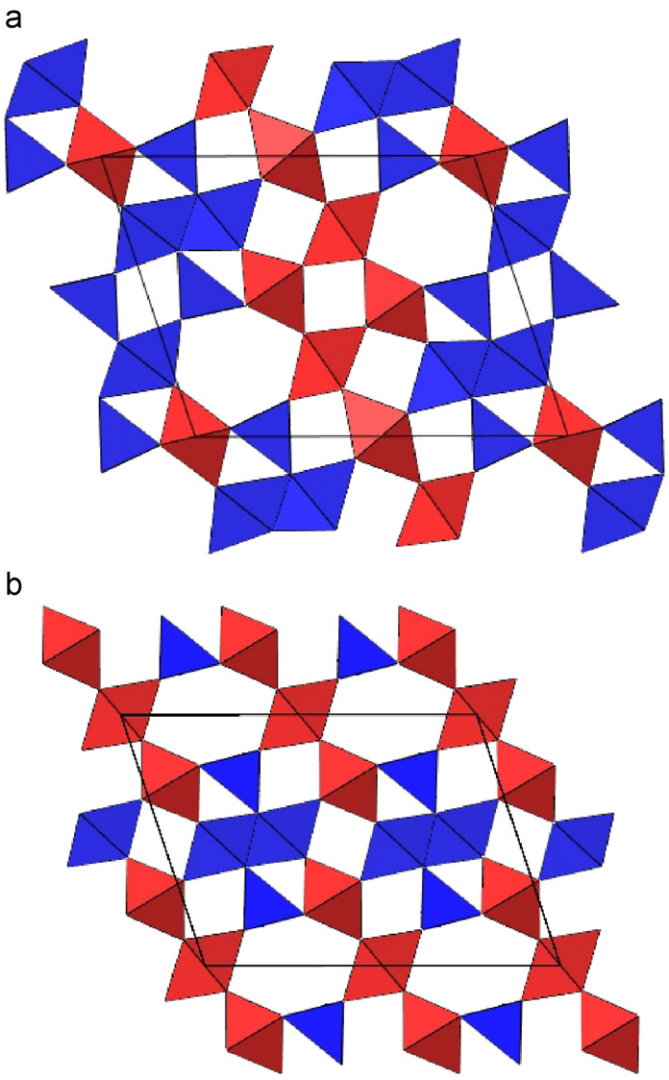

Fig. 5. Two structures of $n = 7$ BGR intergrowths projected along the [010] with the *a*-axis placed horizontally: (a) model of *P*2/*m* structure reported for $Ga_{4-4x}In_{4x}Sn_3O_{12}$ [6] and (b) refined *C*2/*m* structure of $Ga_{3.24}In_{0.76}Sn_{2.4}Ti_{0.6}O_{12}$. Corner-sharing $(Sn/Ti)O_6$ octahedra shown in red. Edge sharing $(Ga,In)O_6$ octahedra and GaO_4 tetrahedra shown in blue.

shows a refinement in which the thermal parameters of the Sn/Ti sites were allowed to refine to negative values with Sn and Ti held fixed at an even distribution on the three sites. Manual placement of the Sn/Ti on different sites when the thermal parameter was held constant did not result in a significantly different fit to the data than that shown in Fig. 4. All of the constrained refinements did, however, confirm the preference of In to reside on the *M*(4) site.

3.3. Structure refinement of $Ga_{3.24}In_{0.76}Sn_{2.4}Ti_{0.6}O_{12}$ ($n = 7$)

Fig. 2b shows the X-ray diffraction pattern for the sample prepared as $Ga_{3.24}In_{0.76}Sn_{2.4}Ti_{0.6}O_{12}$ ($n = 7$). The pattern was indexed to a monoclinic cell, and refinement provided the following lattice parameters: $a = 14.2717(3)$ Å, $b = 3.13(8)$ Å, $c = 10.6288(7)$, $\beta = 108.4057(1)^\circ$. While there are no strong reflections to suggest a primitive unit cell, some of the c-centered reflections do show broadening of what could be reflections allowed by primitive symmetry.

As mentioned previously, two structures are possible for the $n = 7$ BGR intergrowths, as illustrated in Fig. 5. Kahn et al. [3] reported a *C*2/*m* structure for $Ga_4Ge_3O_{12}$, whereas Edwards et al. [6] reported a *P*2/*m* structure for $Ga_{4-4x}In_{4x}Sn_3O_{12}$ based on X-ray diffraction and high-resolution transmission electron microscopy. Using computational modeling, Empie and Edwards [9] reported lattice parameters for *C*2/*m* and *P*2/*m* polymorphs of $Na_{0.8}Ga_{4.8}Ti_{2.2}O_{12}$, an alkali-doped $n = 7$ BGR intergrowth structure.

Given the similarity in composition of the present sample to that reported by Edwards et al. [6], it was anticipated that the current structure would assume *P*2/*m* symmetry. We first attempted to refine the structure using the *P*2/*m* model, but an acceptable fit to the observed data was never achieved. Even in the best fits to the data, the difference plot clearly suggested an incorrect model.

Using a *C*2/*m* symmetry model with the atom positions reported by Empie and Edwards [9] as starting values led to an improved fit to the data. The subsequent refinement was conducted using the same strategy as that described above for the $Ga_{4-4x}In_{4x}Sn_{2-2y}Ti_{2y}O_{10}$ sample. This led to a refinement that rapidly converged and produced much more reasonable structural results.

Table 3
Structural parameters for $Ga_{3.24}In_{0.76}Sn_{2.4}Ti_{0.6}O_{12}$ ($n = 7$)[a]

Atom	Site	*x*	*y*	*z*	U_{iso}*100 Å^2	Occupancy
Sn(1)	2*a*	0	0	0	5.6(2)	1
Sn(2)	4*i*	0.4298(4)	0	0.2692(5)	2.5(2)	0.848(9)
Ti(2)	4*i*	0.4298(4)	0	0.2692(5)	2.5(2)	0.152(9)
Ga(3)	4*i*	0.1440(4)	0	0.4752(4)	8.6(5)	0.59(4)
In(3)	4*i*	0.1440(4)	0	0.4752(4)	8.6(5)	0.41(4)
Ga(4)	4*i*	0.2034(2)	0.5	0.2147(3)	4.6(1)	1
O(1)	4*i*	0.1429(2)	0	0.1402(3)	3.5(2)	1
O(2)	4*i*	0.4639(3)	0	0.1013(4)	4.5(2)	1
O(3)	4*i*	0.0188(3)	0	0.3375(4)	3.7(2)	1
O(4)	4*i*	0.3281(2)	0.5	0.2023(3)	4.3(2)	1
O(5)	4*i*	0.2078(3)	0.5	0.3944(4)	3.4(2)	1
O(6)	4*i*	0.1151(3)	0.5	0.5703(3)	3.7(2)	1
		h k l		R_{wp}		R_p
Bank1		60		0.0443		0.0373
Bank2		30		0.0273		0.0230
Bank3		8		0.0319		0.0310
Totals		98		0.0387		0.0321
χ^2		1.713				

[a] Space group *C*2/*m*, $a = 14.2644(1)$Å, $b = 3.12751(2)$Å, $c = 10.6251(8)$Å, $\beta = 108.405(1)^\circ$.

The $C2/m$ centering leads to a much simpler structure as compared to the $Ga_{4-4x}In_{4x}Sn_{2-2y}Ti_{2y}O_{10}$ ($P2/m$) structure, as there are only two independent Sn/Ti octahedral sites, one Ga/In octahedral site, and one Ga tetrahedral site. Again it was assumed that the Ga tetrahedra did not contain any substituted In atoms due the short bond lengths in this structural element. Contrary to the previous refinement, a strong correlation between the thermal displacement parameter of the Sn/Ti atoms sites was not observed, allowing these two parameters to be refined independently of one another. During the refinement, the Ti occupancy on one of the sites 2a(0,0,0), freely refined to a value not significantly different from zero. Therefore, in the final refinement, this site was assumed to be purely Sn. To test the validity of this assumption, the two independent Sn/Ti sites were constrained to have equal temperature factors, and the site occupancy fractions refined to similar values as before. Relevant structural parameters for this phase are given in Table 3, while interatomic separations derived from the powder data are given in Table 4. As was noted before, the average bond length within the $M(1)$–O_6 octahedra is on average larger than the corresponding separations in the $M(2)$–O_6 octahedra, which further verifies the preferential Ti atom distribution in this structure. The local bonding environment in the $M(3)$–O_6 octahedra is comparable to the same local structure in the $Ga_{4-4x}In_{4x}Sn_{2-2y}Ti_{2y}O_{10}$ ($n = 6$) sample.

As with the refinement of the $n = 6$ structure, the refinement described above led to a composition ($Ga_{3.18}In_{0.82}Sn_{2.69}Ti_{0.31}O_{12}$) different from the as-batched composition of ($Ga_{3.24}In_{0.76}Sn_{2.4}Ti_{0.6}O_{12}$). Additional refinements, conducted with compositional constraints, led to an acceptable fit to the data, $R_{wp} \cong 0.04$ and $\chi^2 = 1.7$, but again resulted in negative isotropic thermal parameters for the Sn/Ti sites. Fig. 6 shows the fit of one such refinement.

Table 4
Bond lengths in $Ga_{3.24}In_{0.76}Sn_{2.4}Ti_{0.6}O_{12}$ ($n = 7$)[a]

Polyhedra	Bond		Number	Length* (Å)
SnO_6	Sn(1)	–O(1)	2	2.111(3)
		–O(2)	4	2.054(3)
$(Sn/Ti)O_6$	Sn(2)/Ti(2)	–O(2)	1	1.992(5)
		–O(3)	2	2.001(4)
		–O(4)	2	2.098(5)
		–O(6)	1	2.002(6)
$(Ga/In)O_6$	Ga(3)/In(3)	–O(3)	1	1.918(6)
		–O(5)	2	2.123(4)
		–O(5)	1	2.131(7)
		–O(6)	2	1.975(4)
GaO_4	Ga(4)	–O(1)	2	1.840(2)
		–O(4)	1	1.824(4)
		–O(5)	1	1.890(5)

[a] Values in parentheses refer to 1 estimated standard deviation in the last digit.

3.4. Structure determination and refinement of $Ga_{3.24}In_{0.76}Sn_4TiO_{16}$

Kahn et al. [3] previously proposed a model for a $C2/m$ ($n = 9$) intergrowth phases, but a detailed structural investigation for any composition has not been reported. Here, we have solved the structure ab-initio using a combination of X-ray and neutron diffraction data. An analysis of X-ray powder diffraction data resulted in a $C2/m$ cell of refined dimensions: $a = 18.1880(6)$ Å, $b = 3.14(7)$ Å, $c = 10.6085(7)$ Å, $\beta = 102.6619(1)^\circ$.

The constrictively short unit cell b length of ~3 Å greatly simplifies the placement of atoms in this structure to $y = 0$ and 0.5. A further simplification of the structure solution is affected by the fact that every known intergrowth structure of this type contains a rutile-type structural element centered on a site of highest symmetry. Therefore, to produce the stoichiometry of this phase, it was postulated that the unit cell would possess Sn/Ti–O_6 octahedra centered on site 2a (0,0,0), two Sn/Ti–O_6, a Ga/In–O_6 octahedra residing on 4i ($x, 0, z$) sites, and a Ga/In–O_4 tetrahedron on the same type of site.

Using the ab-initio structure determination program FOX [14], the low angle region of the X-ray diffraction data for this sample was used to determine the approximate cation positions. The structure was modeled via a rigid-body approach, wherein a

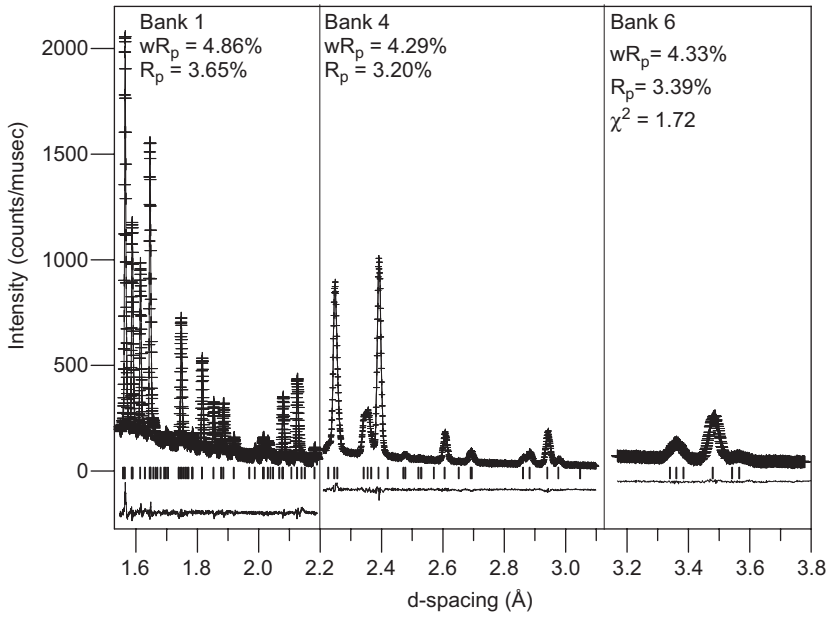

Fig. 6. Observed (+), calculated (line), and difference patterns for $Ga_{3.24}In_{0.76}Sn_{2.4}Ti_{0.6}O_{12}$. Rietveld analysis of neutron diffraction data was conducted using hard and soft constraints to maintain original composition.

single Sn–O_6 octahedron was constrained to reside on a 2*a* site, and the remainder of the rigid-bodies (three octahedra and one tetrahedron) was assigned random positions of the type: $(x, 0, z)$, and the *y* value of the fractional coordinates was constrained to be zero. The only degrees of freedom afforded to the rigid-body was translation ($y = 0$), rotation, and uniform expansion/contraction, with the exception of the Sn–O_6 octahedra, centered at $(0, 0, 0)$, which was not permitted to translate. Nevertheless, this heavily constricted approach resulted in a very rapid solution for the cation positions, which were utilized as the starting model for the neutron diffraction data.

There remained a total of eight oxygen atom positions to be determined, and by use of the Le Bail method [15] in the GSAS program suite, structure factors from the neutron data were extracted, and a Patterson synthesis was conducted on the extracted structure factor moduli. Such an approach is possible in that all atom positions will have an apparent scattering density greater than zero (the neutron scattering length for Ti is negative, but the amount of Ti present on any of the rutile-like sites is not significant enough to create an effective negative neutron scattering density). The generation of Patterson maps from powder data usually leads to ill-defined maps as compared to those derived from single-crystal data, however, a forehand knowledge of the cation positions greatly aided in the interpretation of the Patterson maps generated from the neutron powder data, and six of the eight oxygen atom positions required by the stoichiometry of the sample were readily identified. As the basic structural chemistry of these phases is known insofar as they are comprised of elements from each of the rutile and β-gallia parent phases, the remaining two oxygen atom positions, though not seen in the Patterson map due to peak overlap, were postulated on the basis of expected bond lengths.

Using the starting model generated from the X-ray data and Patterson synthesis from neutron data, the structure was imported into GSAS, and despite the fact that the fractional coordinates of the atoms were only approximate, a very convincing fit to the observed pattern prior to refinement was obtained. Using procedures as described for the prior two data sets, the refinement rapidly converged. All three Sn/Ti atom positions were constrained to have identical thermal displacement parameters to reduce the effects of correlation amongst these parameters, the site occupancy values, and the scale factor. The relevant structural parameters for this structure are listed in Table 5, and the corresponding interatomic separations inferred from the refined parameters are given in Table 6. The agreement indices ($\chi^2 = 2.131$, $R_{wp} = 0.0389$) in conjunction with the self-consistency of the calculated interatomic separations as compared to the other structures lends support for the proposed structural model. A perspective view in the (010) reflection plane of this structure is offered as Fig. 7. The final model is consistent with that proposed by Kahn et al. [3] for $Ga_4Ti_5O_{16}$. Moreover, scrutiny of HRTEM images for a sample of $Ga_{4-4x}In_{4x}Sn_5O_{16}$ (see Fig. 9 in Ref. [6]) further reveals that the location of the tunnels in the unit cell is identical to the arrangement shown in Fig. 7.

Table 5
Structural parameters for $Ga_{3.24}In_{0.76}Sn_4TiO_{16}$ ($n = 9$)[a]

Atom	Site	*x*	*y*	*z*	U_{iso}*100 Å^2	Occupancy
Sn(1)	2*a*	0	0	0	5.3(2)	0.881(9)
Ti(1)	2*a*	0	0	0	5.3(2)	0.119(9)
Sn(2)	4*i*	0.0581(3)	0.5	0.3206(5)	5.3(2)	0.913(8)
Ti(2)	4*i*	0.0581(3)	0.5	0.3206(5)	5.3(2)	0.087(8)
Sn(3)	4*i*	0.1154(3)	0	0.6390(6)	5.3(2)	0.832(7)
Ti(3)	4*i*	0.1154(3)	0	0.6390(6)	5.3(2)	0.168(7)
Ga(4)	4*i*	0.1685(3)	0.5	−0.0507(4)	3.9(6)	0.27(4)
In(4)	4*i*	0.1685(3)	0.5	−0.0507(4)	3.9(6)	0.73(4)
Ga(5)	4*i*	0.2130(1)	0	0.2566(4)	4.5(1)	1
O(1)	4*i*	0.0350(3)	0	0.1954(4)	4.2(2)	1
O(2)	4*i*	0.1498(3)	0	−0.1646(4)	5.8(2)	1
O(3)	4*i*	0.2150(3)	0	0.0797(5)	5.0(3)	1
O(4)	4*i*	−0.0726(3)	0.5	0.0069(4)	4.9(2)	1
O(5)	4*i*	0.1676(2)	0.5	0.2837(4)	5.1(2)	1
O(6)	4*i*	0.3081(2)	0	0.3582(4)	5.9(2)	1
O(7)	4*i*	−0.0479(3)	0.5	0.3516(4)	3.9(2)	1
O(8)	4*i*	0.0909(2)	0	0.4464(4)	4.1(2)	1
		h k l		R_{wp}		R_p
Bank1		79		0.0444		0.0366
Bank2		41		0.0284		0.0229
Bank3		10		0.0307		0.0269
Totals		130		0.0389		0.0313
χ^2		2.131				

[a] Space group *C*2/*m*, $a = 18.1754(2)$Å, $b = 3.13388(3)$Å, $c = 10.60671(9)$Å, $\beta = 102.657(1)^\circ$.

Table 6
Bond lengths in $Ga_{3.24}In_{0.76}Sn_4TiO_{16}$ ($n = 9$)

Polyhedra	Bond	Number	Length (Å)
Sn/Ti)O_6	Sn(1)/Ti(1)		
	–O(1)	2	2.030(4)
	–O(4)	4	2.0604(34)
(Sn/Ti)O_6	Sn(2)/Ti(2)		
	–O(1)	2	2.037(4)
	–O(5)	1	2.110(7)
	–O(7)	1	2.025(7)
	–O(8)	2	2.059(4)
(Sn/Ti)O_6	Sn(3)/Ti(3)		
	–O(2)	1	2.039(7)
	–O(6)	2	2.091(5)
	–O(7)	2	2.005(5)
	–O(8)	1	1.993(7)
(Ga/In)O_6	Ga(4)/In(4)		
	–O(2)	2	1.963(4)
	–O(3)	2	2.138(4)
	–O(3)	1	2.205(8)
	–O(4)	1	1.899(7)
GaO_4	Ga(5)		
	–O(3)	1	1.885(6)
	–O(5)	2	1.8229(28)
	–O(6)	1	1.826(5)

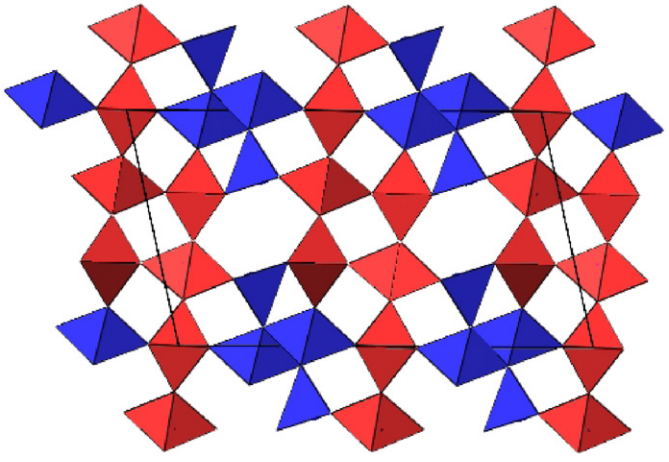

Fig. 7. Structure of $Ga_{3.24}In_{0.76}Sn_4TiO_{16}$ ($n = 9$, *C*2/*m*) projected along [010] with the *a*-axis placed horizontally. Corner-sharing (Sn/Ti)O_6 octahedra shown in red. Edge sharing (Ga,In)O_6 octahedra and GaO_4 tetrahedra shown in blue.

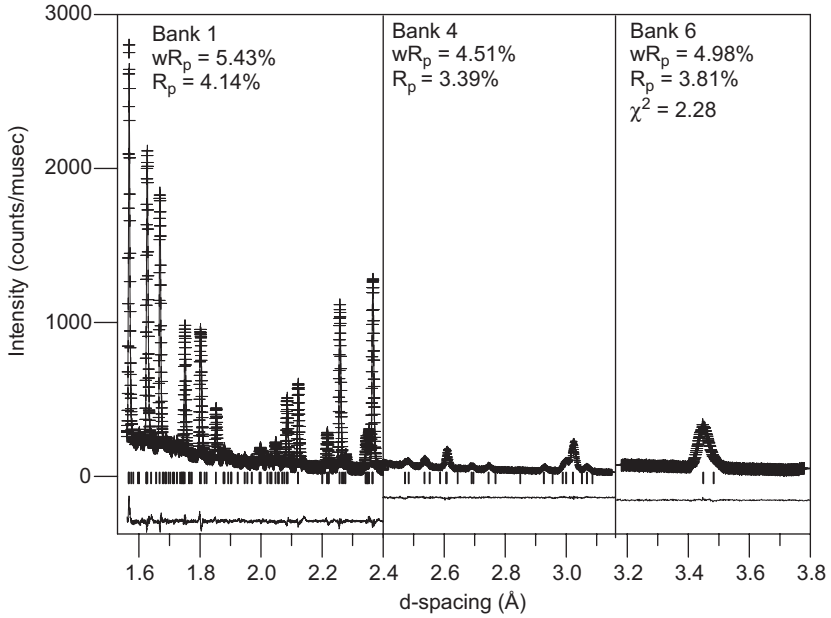

Fig. 8. Observed (+), calculated (line), and difference patterns for $Ga_{3.24}In_{0.76}Sn_4TiO_{16}$. Rietveld analysis of neutron diffraction data was conducted using hard and soft constraints to maintain original composition.

As with the previous structures, the reported refinement does not accurately reproduce the starting composition of the sample, $Ga_{2.54}In_{1.46}Sn_{4.37}Ti_{0.63}O_{16}$ vs. $Ga_{3.24}In_{0.76}Sn_4TiO_{16}$. Additional refinements were conducted with various hard and soft constraints to maintain the as-batched compositions. As with previous refinements, the constrained refinements led to acceptable fits, but often resulted in negative isotropic thermal parameters for some or all of the Sn/Ti sites, depending on which constraints were used. Fig. 8 shows an example of a refinement in which Sn and Ti were evenly distributed across the Sn/Ti sites and in which the isothermal parameters were allowed to refine independently to negative values. When the isothermal parameters of the Sn/Ti sites were constrained to be equal to each other, the restrained Sn/Ti ratios refined to values which were not significantly different from each other and provided a fit comparable to that shown in Fig. 8.

4. Conclusions

Samples expressed as $(Ga,In)_4(Sn,Ti)_{n-4}O_{2n-2}$, $n = 6$, 7, and 9 were prepared by solid-state reaction and characterized. For samples prepared with $n = 6$ and 7, only a few compositions with varying ratios of Ga:In and Sn:Ti were found to be phase pure. For samples prepared with $n = 9$, or $Ga_{4-4x}In_{4x}Sn_{5-5y}Ti_{5y}O_{16}$, most compositions prepared with $0.17 \leqslant x \leqslant 0.35$ and $0 \leqslant y \leqslant 0.4$ were phase pure.

The structures of three phases were refined using neutron powder diffraction data. The $n = 6$ phase $Ga_{3.24}In_{0.76}Sn_{1.6}Ti_{0.4}O_{10}$ is isostructural with $Ga_{2.8}In_{1.2}Sn_2O_{10}$, crystallizing in $P2/m$ with $a = 11.5934(3)$ Å, $b = 3.12529(9)$ Å, $c = 10.6549(3)$ Å, $\beta = 99.146(1)^\circ$. The $n = 7$ phase $Ga_{3.24}In_{0.76}Sn_{2.4}Ti_{0.6}O_{12}$ crystallizes in $C2/m$ with $a = 14.2644(1)$ Å, $b = 3.12751(2)$ Å, $c = 10.6251(8)$ Å, $\beta = 108.405(1)^\circ$. It is isostructural with the reported structure of $Ga_3Ge_4O_{12}$ but different from the $Ga_{4-4x}In_{4x}Sn_3O_{12}$ solid solution which crystallizes in $P2/m$. The $n = 9$ phase $Ga_{3.16}In_{0.84}Sn_4TiO_{16}$ also crystallizes in $C2/m$ with $a = 18.1754(2)$ Å, $b = 3.13388(3)$ Å, $c = 10.60671(9)$ Å, $\beta = 102.657(1)^\circ$. All of the structures are similar in that they possess distorted hexagonal tunnels parallel to the [010] vector.

Acknowledgments

This work was supported by the National Science Foundation (DMR-0093690). Neutron diffraction data were obtained from the Intense Pulse Neutron Source at Argonne National Laboratory, which is funded by the US Department of Energy under Contract W-31-109-ENG-38.

References

[1] S. Kamiya, R.J.D. Tilley, J. Solid State Chem. 22 (1977) 205–216.
[2] L.A. Bursill, G.G. Stone, J. Solid State Chem. 38 (1981) 149–157.
[3] A. Kahn, V. Agafonov, D. Michel, M. Perez y Yorba, J. Solid State Chem. 65 (1986) 377–382.
[4] M.B. Varfolomeev, A.S. Mironova, T.I. Dudina, N.D. Koldashov, Zh. Neorg. Khim. 20 (1975) 3140–3141.
[5] D.D. Edwards, T.O. Mason, J. Am. Ceram. Soc. 81 (12) (1998) 3285–3292.
[6] D.D. Edwards, T.O. Mason, W. Sinkler, L.D. Marks, K.R. Poeppelmeier, Z. Hu, H.D. Jorgensen, J. Solid State Chem. 150 (2000) 294–304.
[7] G.V. Chandrashekar, A. Bednowitz, S.J. La Placa, in: P. Vashishta, J.N. Mundy, G.K. Shenoy (Eds.), Fast Ion Transport in Solids, North-Holland, Amsterdam, 1979, p. 447.
[8] D.D. Edwards, N.H. Empie, N. Meethong, J. Amoroso, Solid State Ionics 177 (2006) 1897–1900.
[9] N.H. Empie, D.D. Edwards, Solid State Ionics 177 (1–2) (2006) 77–87.
[10] A.C. Larson, R.B. Von Dreele, Los Alamos National Laboratory Report LAUR, 2000, pp. 86–748.
[11] B.H. Toby, J. Appl. Crystallogr. 34 (2001) 210–213.
[12] T. Hahn, International Tables for Crystallography, second ed., D Reidel Publication Company, Boston, NY, USA, 1987.
[13] M. Park, T.E. Mitchell, A.H. Heuer, J. Am. Ceram. Soc. 58 (1–2) (1975) 43–47.
[14] V. Favre-Nicolin, V.R. Cerny, J. Appl. Crystallogr. 34 (6) (2002) 734–743.
[15] A. Le Bail, A.H. Duroy, J.L. Fourquet, Mater. Res. Bull. 23 (1988) 447–452.